Ecotoxicology and Environmental Safety 184 (2019) 109622

Contents lists available at ScienceDirect

Ecotoxicology and Environmental Safety

journal homepage: www.elsevier.com/locate/ecoenv

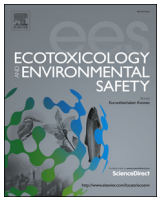

Ecological and health risk assessment of exposure to atmospheric heavy metals

Abdolmajid Gholizadeh[a], Mahmoud Taghavi[b], Alireza Moslem[c], Ali Asghar Neshat[a], Moslem Lari Najafi[d], Ahmad Alahabadi[e], Ehsan Ahmadi[f,g], Hamideh Ebrahimi aval[h], Akbar Ahmadi Asour[i], Hossein Rezaei[e], Sedighe Gholami[e], Mohammad Miri[e,*]

[a] Esfarayen Faculty of Medical Sciences, Esfarayen, Iran
[b] Department of Environmental Health, School of Public Health, Gonabad University of Medical Sciences, Gonabad, Iran
[c] School of Medicine, Sabzevar University of Medical Sciences, Sabzevar, Iran
[d] Food, Drug and Cosmetics Safety Research Center, Kerman University of Medical Sciences, Kerman, Iran
[e] Non-Communicable Diseases Research Center, Department of Environmental Health, School of Public Health, Sabzevar University of Medical Sciences, Sabzevar, Iran
[f] Department of Environmental Health Engineering, School of Public Health, Kashan University of Medical Sciences, Kashan, Iran
[g] Students' Scientific Research Center (SSRC), Tehran University of Medical Sciences, Tehran, Iran
[h] Department of Health Education and Health Promotion, School of Public Health, Sabzevar University of Medical Sciences, Sabzevar, Iran
[i] Department of Occupational Health, School of Public Health, Sabzevar University of Medical Sciences, Sabzevar, Iran

ARTICLE INFO

Keywords:
Heavy metals
Health risk assessment
Ecological risk assessment
Air pollution
Pinus eldarica

ABSTRACT

In the present study, we assessed the concentration of airborne HMs (Zn, Cu, Pb, and Cd) and their probable sources using the bark of *Pinus eldarica* as a bio-indicator. Hence, 47 tree bark samples were harvested according to the land uses and biomonitoring techniques in the city of Yazd, Iran. The potential health risks in 13 age groups, ecological risk, as well as the possible relationship between HM concentrations and traffic indicators, were evaluated. The order of average HM concentrations in the *P. eldarica* bark samples was as Zn > Pb > Cu > Cd. The mean values of non-carcinogenic risks of all HMs in entire age groups were within secure range (HQ < 1); however, the carcinogenic risk of Cd was higher than the allowed level (TCR > 1×10^{-6}). About Pb, it was in the safe level. The main element causing potential ecological risks was Cd, indicating moderate to very high ecological risk in most of the study areas. There was an inverse significant association between distance from major roads and Pb concentration (β = −0.011 95% confidence interval (CI): 0.022, −0.0001). All HMs in bark samples render the negative Moran's index, representing a random spatial distribution pattern. Besides, according to principal component analysis (PCA), the first component accounted for 36.55% of the total variance, dominated by Cd, Pb, Cu, and Zn, respectively, and characterized by vehicle and industrial emissions. Our results infer that industrial activities and traffic are the main sources of HMs pollution in urban environments that should be considered by decision-makers.

1. Introduction

Along with the preeminent dependency of man on various industries, modern technologies, and fossil fuels, the exposure to environmental pollution is also increasing (Ghaffari et al., 2017; Serbula et al., 2012). It has been estimated 35,000 people die each year owing to air pollution in the United States (Bell et al., 2011). Of the numerous air pollutants, heavy metals (HMs) have received great attention due to their non-biodegradability, as well as physiological and disruptive effects on living organisms even at low concentrations (Gholizadeh et al., 2018). Generally, direct or indirect methods can be used for measuring HMs pollution in the ambient air. Using a direct method, HM concentrations were measured by air sampling during a short period (e.g., one day, week or month) (Mohsen et al., 2018; Olawoyin et al., 2018). Using indirect method, ambient HM pollution was measured in rainwater (Uchiyama et al., 2019), topsoil or using a bioindicator like leave and bark of plants (Miri et al., 2016). However, major focus has been put on indigenous plants as long-term air pollution bioindicators over the last four decades, mainly due to simpler sampling, ease of implementation, slight cost, low risk, and higher concentrations of metals (Gupta et al., 2016; Sawidis et al., 2011; Zhao et al., 2012). Bioindicator generally refers to organisms providing quantitative information to the

* Corresponding author. Sabzevar University of Medical Sciences, Sabzevar, Iran.
E-mail address: M_miri87@yahoo.com (M. Miri).

https://doi.org/10.1016/j.ecoenv.2019.109622
Received 12 March 2019; Received in revised form 20 August 2019; Accepted 28 August 2019
Available online 06 September 2019
0147-6513/

researchers about the environment quality (Moreira et al., 2016; Parmar et al., 2016).

Heavy metals present in the air can accumulate in the leaf and bark of plants (Birke et al., 2018; Janta and Chantara, 2017), largely depending on plant characteristics (including growth rate and biomass) and the amount of HMs present in the soil. Ample surface and rendering sticky sap of some tree barks provide high adsorption capability (Carvalho-Oliveira et al., 2017; Guéguen et al., 2012; Minganti and Drava, 2018). Moreover, the transferring possibility of HMs from the root to the trunk is negligible or unlikely (Martin et al., 2018). Antoniadis et al. (2017) and Roque-Álvarez et al. (2018) reported that HMs uptake into a tree from the soil is unlikely since these elements have low plant mobility. Therefore, the presence of these deposits in the tree bark can be attributed significantly to the adsorption of these pollutants from the air (Birke et al., 2018). Hence, tree bark can be an ideal cumulative biological indicator of long-term air pollution (Birke et al., 2018; Janta and Chantara, 2017).

Previous studies investigated the health risk of exposure to ambient HMs using particulate matter (PM) sampling for a limited period (e.g. two weeks) (Chen et al., 2015); however, the available evidence about the health risk assessment of long-term exposure to ambient HMs is still scarce. To our knowledge, this is the first study on the probabilistic health risk assessment of long-term exposure to ambient HMs using bark samples as bioindicator. Given the previous studies, the amount of metals in the outer layer of the bark has a high accuracy in the evaluation of long-term air pollution (Birke et al., 2018; Cocozza et al., 2016; Kandziora-Ciupa et al., 2016; Miri et al., 2017b; Parmar et al., 2016; Sawidis et al., 2011), it can be expected that the calculated risk level in this study is closer to the actual value than the former studies carried out based on short-term measurements.

This study aimed to measure ambient HMs concentration using *Pinus eldarica* barks as a bioindicator of long-term exposure to air pollution. Ecological risks of HMs pollution in the study area, as well as their health risks and sensitivity analyses, were assessed for 13 age groups (from birth to ≤ 80 years old) using a probabilistic approach. Finally, source identification of HMs was investigated through spatial and statistical techniques.

2. Material and methods

2.1. Study area

This study was conducted in the Yazd, a metropolitan city in the center of Iran, located at a longitude between 54.24° and 54.42° and latitude of 31.79°–31.95°, and elevation about 1190–1300 m above mean sea level. This city with an area of 2491 km^2 has a population about 650,000, where is one of the driest regions in Iran with the average temperature and annual precipitation of 20.3 °C and 50 mm, respectively (Miri et al., 2017b). The dominant wind direction in the Yazd province is generally northwest to the southeast, which blows particularly in mid-spring to the early autumn period. There are many industrial towns around this city (e.g. steel, ceramic tile, and pipe industries) and has a traffic density ranged between 5000 and 100,000 vehicles per day. Fig. 1 depicts the study area, sampling locations, major roads, airport, bus terminal, and the industrial regions.

2.2. Bioindicator selection, sampling, and preparation

According to the different land uses and distance from air pollution resources, such as bus terminals, airport, main roads, and high-populated areas, 47 samples extended from various microenvironments were harvested. The sampling point coordinates were determined using a Global Positioning System (GPS) in the universal transfer Mercator (UTM) coordinate system (Fig. 1).

Pinus eldarica was selected as the HMs bioindicator because it is one of the most common species in the studied area, usually planted along main roads, residential and industrial areas, and suburbs for landscaping and shading. Those trees were selected that had the average age between 10 and 15 years old because these must have a soft bark, and the HMs accumulation on the bark is not related to tree age within this range (Janta and Chantara, 2017; Janta et al., 2016). For samples harvesting, we followed the methodology of Birke et al. (2018) with a few modifications. Samples were collected from about 1.5 m above ground level (50 g each sample) using a razor blade and placed in plastic bags. The samples did not have any defections (bird dropping, pesticide treatment, and insect infestation), and did not receive further treatment until receiving to the laboratory. The sampling process was conducted during late spring of 2017 after a 10-day rainless period. Samples were carefully cleaned using a brush to remove external material. Their outer layers were scratched using a clean knife, powdered using a laboratory mill, and subsequently dried at lab temperature.

HM contents were extracted by acid digestion method (Şen et al., 2015). Due to technical and budget limitations, this study has measured just four HMs (zinc (Zn), copper (Cu), lead (Pb) and cadmium (Cd)). HM concentration was measured using a graphite furnace atomic absorption spectrophotometer (GF-AAS) (Varian SpectrAA.20 Plus, Varian, Inc.). Each sample was injected thrice using an automatic sampler, and the average concentration was used for future data analyses. A blank in the same condition was considered for every 10 samples. The limit of detection (LOD) of each element was determined three times. Standard deviation (SD) of eight blank repetitions and amount of recovery were 80–120%.

2.3. Risk assessment

2.3.1. Human risk assessment

Risk assessment is an overall process or approach, used to identify health impacts and risk factors of exposing to a specific pollutant through different pathways (Zhao et al., 2014). Three main routes of chemical daily intake (CDI, mg kg^{-1} day^{-1}) of air HMs are: (1) direct ingestion of particles or gases existed in the air (CDI_{ing}); (2) inhalation of suspended particles through mouth and nose (CDI_{inh}); and (3) daily absorption of HMs through skin (CDI_{dermal}). Since the HMs studied here have carcinogenic and non-carcinogenic effects (Luo et al., 2012), both risks of these exposure routes were assessed in the 13 age groups in detail (from birth to ≤ 80 years old) (Table 1). CDI_{ing}, CDI_{inh}, and CDI_{dermal} were estimated as:

$$CDI_{ing} = C \times \frac{IRing \times EF \times ED}{BW \times AT} \times 10^{-6} \quad (1)$$

$$CDI_{dermal} = C \times \frac{SA \times AF \times ABS_d \times EF \times ED}{BW \times AT} \times 10^{-6} \quad (2)$$

$$CDI_{inh} = C \times \frac{IRinh \times ET \times EF \times ED}{BW \times AT} \quad (3)$$

Moreover, hazard index (HI) and total carcinogenic risk (TCR) for each HM were calculated using Eqs. (4)–(7) (Luo et al., 2012; Zhao et al., 2014):

$$carcinogenic\ risk = CDI_{ing/dermal/inh} \times CSF \quad (4)$$

$$TCR = \sum \text{risk} = \text{CDI}_{\text{ing}} \times \text{CSF}_{\text{ing}} + \text{CDI}_{\text{inh}} \times \text{IUR} + \text{CDI}_{\text{dermal}} \times \text{CSF}_{\text{ing}}/ABS_{GI} \quad (5)$$

$$Hazard\ quotient\,(HQ) = CDI_{ing/dermal}/RfD + \text{CDI}_{ihl}/RfC \quad (6)$$

$$HI = \sum HQ = HQ_{ing} + HQ_{inh} + HQ_{dermal} \quad (7)$$

The parameters and their values included in the models are presented in Table 1. As a rule, the higher values of CDI than RfD mean the higher level of concern. Thus, HQ ≤ 1 and HQ > 1 suggest improbability and probability of detrimental health effects, respectively. The excess carcinogenic risks lower than 10^{-6} are considered negligible,

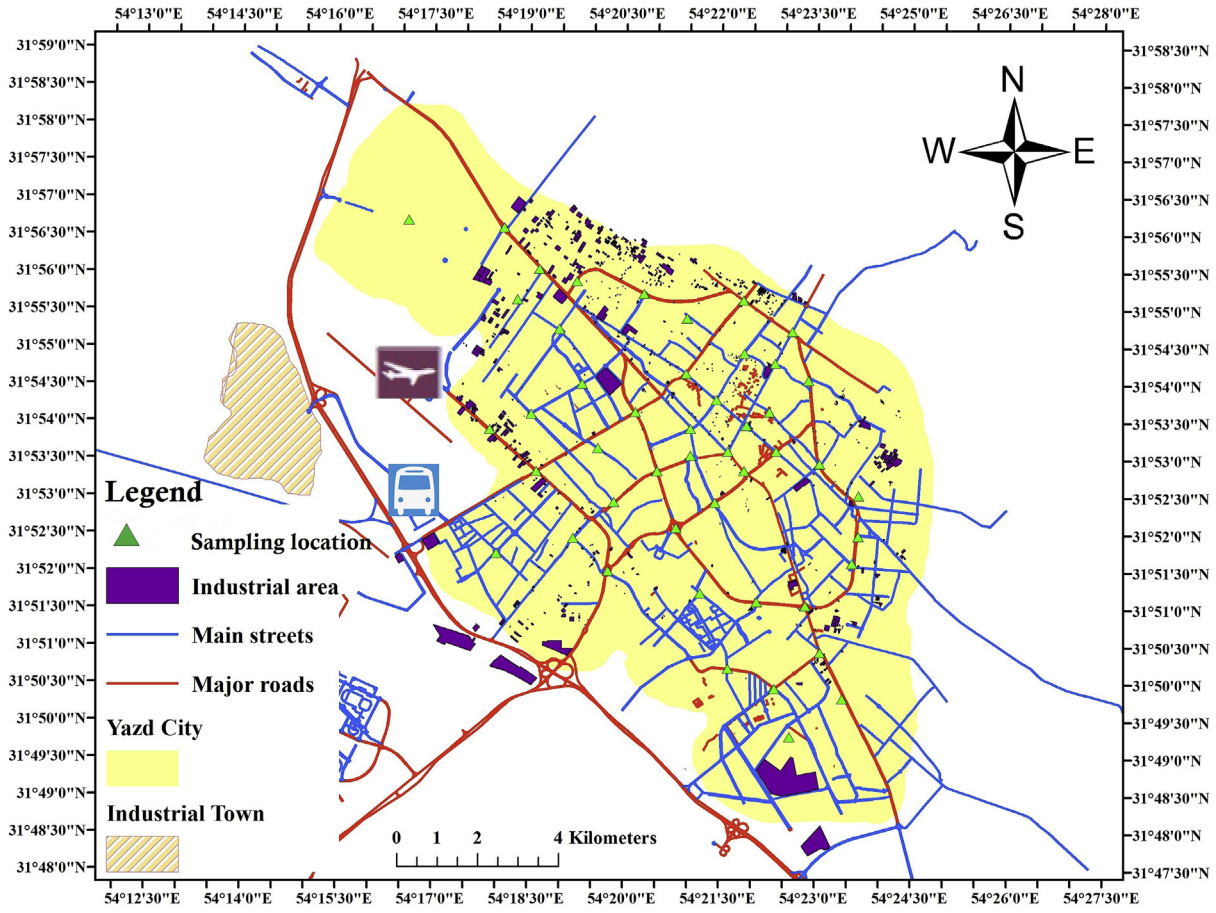

Fig. 1. Geographical location of study area, Yazd, Iran.

and risks above 10^{-4} are unacceptable by most international regulatory agencies (Luo et al., 2012). The value 10^{-6} is also considered the carcinogenic target risk by USEPA (USEPA, 2011).

2.3.2. Monte Carlo simulations and sensitivity analysis

If the single-point value of a variable is used to calculate the risk for a population, it may increase the probability of interference, error, and eventually the result uncertainty. Therefore, here, Monte Carlo simulations were used to minimize uncertainties associated with human health risks and obtain a probabilistic approximation of a model (Huang et al., 2017; Keramati et al., 2018). The effective doses of HMs were estimated using Monte Carlo simulation in the Crystal Ball software (Version 11.1.2.4, Oracle, Inc., USA). Finally, the results were demonstrated with different degrees of confidence intervals from 1 to 99%.

Sensitivity analysis was accomplished on the Monte Carlo simulation results with 100,000 trails to order the variables that have the greatest impact on risk assessment results. Besides, that parameter which has a higher coefficient represents the greater share in risk uncertainty (Miri et al., 2018a).

2.3.3. Ecological risk assessment

To obtain ecological risk, ordinary kriging (OK) model was employed using ArcGIS 10.2 software (ESRI, Redlands, CA), and the HMs distribution pattern throughout the study area was illustrated (Figs. S1–S4 of supplemental materials). OK model was fitted for all HMs based on the best semivariogram, and lowest root mean square error (RMSE). Then, potential ecological risk (E_r^i) and ecological risk index (RI) of HMs assessed the sensitivity of different biological communities to toxic metals. The degree of HMs pollution in the study area was estimated using the raster calculator of map algebra tool (Barkett and Akün, 2018). The integrated RI is calculated as:

$$RI = \sum_{i=1}^{n} E_r^i \tag{8}$$

The E_r^i amount of an HM is calculated as follows:

$$E_r^i = T_r^i \times C_f^i \tag{9}$$

where T_r^i is toxic response factor for a given substance, which for Zn, Cu, Cd, and Pb are 1, 5, 30 and 5, respectively (Guo et al., 2010; Hakanson, 1980). C_f^i is the contamination factor; calculated as the concentration of element i in bark sample, divided by its concentration in sample of reference area. Reference samples were obtained from a non-polluted area with 10 km distance from the city. Eventually, the risk level was categorized as shown in Table S1 of Supplemental materials.

2.4. Sources identification

2.4.1. Spatial autocorrelation model

Spatial autocorrelation analysis (Global Moran's I) was utilized in the GIS environment to measure feature similarity. This tool evaluates the pattern distribution (clustered, dispersed, or random) according to a set of features and associated attributes. It also calculates the Moran's index value as well as Z-score and p-value, evaluating the significance of that index. In general, Moran's I value near +1.0 indicates the unipolar or clustering pattern; a zero value represents that values are randomly distributed across the study area pattern, and an index value near −1.0 suggests a dispersed pattern (Gholizadeh et al., 2017). The Global Moran's I can be calculated as (Dong and Liang, 2014;

Table 1
Variables and their values for the estimation of human exposure to air heavy metals.

Parameter	Age groups (year)													Reference
	< 1	1 to < 2	2 to < 3	3 to < 6	6 to < 11	11 to < 16	16 to < 21	21 to < 31	31 to < 51	51 to < 61	61 to < 71	71 to < 81	≥81	
Inhalation rate (IR_{inh}) (m^3 day^{-1})	5.4	8	8.9	10.1	12	15.2	16.3	15.7	16	15.7	14.2	12.9	12.2	USEPA (2011)
Ingestion rate (IR_{ing}) (mg day^{-1})	30	60	60	60	60	60	60	30	30	30	30	30	30	USEPA (2011)
Body weight (BW)(kg)	9.2	11.4	13.8	18.6	31.8	56.8	71.6	80	80	80	80	80	80	USEPA (2011)
Exposure duration (ED) (year)	1	1	1	3	5	5	5	49	49	49	49	49	49	USEPA (2011)
Exposure frequency (EF) (day $year^{-1}$)	350	350	350	350	350	350	350	350	350	350	350	350	350	USEPA (2011)
Averaging time (AT) (day)	350	350	350	1050	1750	1750	1750	17,150	17,150	17,150	17,150	17,150	17,150	USEPA (2011)
skin adherence factor (AF) (mg cm^{-2})	0.2	0.2	0.2	0.2	0.2	0.2	0.07	0.07	0.07	0.07	0.07	0.07	0.07	USEPA (2011)
Total body skin surface area (SA) (m^2)	0.45	0.53	0.61	0.76	1.08	1.59	1.84	1.93	1.99	2	1.98	1.91	1.80	USEPA (2011)
Ingestion cancer slope factor (CSF) (mg kg^{-1} day^{-1})	8.5×10^{-3} for Pb (RAIS)													USDoE (2011)
Inhalation reference concentration (RfC) (mg m^{-3})	1×10^{-5} for Cd													USDoE (2011)
Dermal absorption factor (ABS_d)	0.001 for all elements													USDoE (2011)
Gastrointestinal absorption factor (ABS_{GI})	0.025 for Cd and 1 for other elements													USDoE (2011)
Oral reference dose (RfD) (mg kg^{-1} day^{-1})	1×10^{-3} for Cd, 3.5×10^{-3} for Pb, 4×10^{-2} for Cu and 3×10^{-1} for Zn													USDoE (2011)
inhalation unit risk (IUR) (μg m^{-3})	1.8×10^{-3} for Cd and 1.2×10^{-5} for Pb,													USDoE (2011)

Kanaroglou et al., 2013; Miri et al., 2018b):

$$I = \frac{n}{S_0} \frac{\sum_{i=1}^{n} \sum_{j=1}^{n} w_{i,j} z_i z_j}{\sum_{i=1}^{n} z_i^2} \quad (10)$$

$$S_0 = \sum_{i=1}^{n} \sum_{j=1}^{n} w_{i,j} \quad (11)$$

where (n) is the total number of features, (S_0) is the sum of all spatial weights, z_i indicates the deviation of an attribute for feature i from its mean ($x_i - X$), and $w_{i,j}$ is the spatial weight between feature i and j (Dormann et al., 2007).

Z_I-score is calculated as follows:

$$z_I = \frac{1 - E[I]}{\sqrt{V[I]}} \quad (12)$$

where E[I] and V[I] are equal to $-1/(n-1)$ and $E[I^2] - E[I]^2$, respectively.

2.4.2. Statistical analyses

Data distribution was performed using Shapiro-Wilk test. To identify the possible source and relationship between HMs, Principal component analysis (PCA), and Spearman's rank correlation coefficients were applied using SPSS Package version 24.0 for Windows. PCA is an effective analytical tool for minimizing a set of main variables and extracting a few hidden factors to analyze the relationships between observed variable and samples (Tipping and Bishop, 1999; Viana et al., 2006; Wold et al., 1987).

In addition, the relationship between the HM concentrations and traffic indicators was assessed using linear regression, including the distance from the nearest major roads and total road length around sampling stations in buffers of 100, 300, and 500 m (Dirgawati et al., 2016). The significance level for all models was 0.05.

3. Results and discussion

3.1. HMs concentration in bark samples

The mean HM concentrations in P. eldarica's bark samples are shown in Fig. S1, Supplemental materials. The results indicate that the Zn concentrations (Ave. 28.27 mg kg^{-1}) were higher than others. The median (interquartile range (IQR)) of Zn was 25.71 (12.60) mg kg^{-1}. This value for Cu, Pb, and Cd was 0.92 (3.47), 3.90 (2.77) and 1.20 (0.35) mg kg^{-1}, respectively. The orders of average concentrations of HMs in the study area were as Zn > Pb > Cu > Cd. Other studies also reported a higher proportion of Zn in the tree bark as compared to other HMs (Chabukdhara and Nema, 2013; Moreira et al., 2016). Further, our results are consistent with the findings of Norouzi et al. (2015), who used the tree leaves for biomonitoring of dust-borne HMs. The higher Zn concentrations in the study area can be attributed to the local geochemistry and industrial activities (Chen et al., 2005; Hirshon et al., 2008; Sponza and Karaoğlu, 2002). Apeagyei et al. (2011) reported that the majorities of Cu, Pb, and Zn in urban environments were emitted from anthropogenic sources such as traffic activities. However, the Pb concentration in the study area was within the safe range (5–10 mg kg^{-1}) mentioned by Kabata-Pendias (2010).

Spatial distribution of studied HMs is presented in Figs. S2–S5 of Supplemental materials. Accordingly, there was an increasing trend in Zn and Cu concentrations from the west towards the city center. The highest concentrations of Cu were near to beltway, airport, terminal, and industrial town in the west and northwest of studied area (Fig. S2 of Supplemental materials). The high concentrations of Zn were observed in center and southwest, although the maximum concentration was in industrial part of the city (Fig. S3 of Supplemental materials). About Pb, higher concentrations were observed in the center and southeast of the city, where, there are main highways and high traffic density. The Pb

Table 2
Mean (standard deviation) of carcinogenic and non-carcinogenic risk of exposure to heavy metals in different age groups.

		Age group											
		Birth to < 1	1 to < 2	2 to < 3	3 to < 6	6 to < 11	11 to < 16	16 to < 21	21 to < 31	31 to < 51	51 to < 61	61 to < 71	71 to < 81	81 and older
Zn	HQ_{ing}	3.16E-4	5.03E-4	4.12E-4	3.06E-4	1.78E-4	1.00E-4	7.91E-5	3.53E-5	3.55E-5	3.52E-5	3.53E-5	3.52E-5	3.53E-5
		(1.28E-4)	(1.92E-4)	(1.56E-4)	(1.12E-4)	(6.28E-5)	(3.59E-5)	(2.81E-5)	(1.30E-5)	(1.33E-5)	(1.28E-5)	(1.31E-5)	(1.30E-5)	(1.28E-5)
	HQ_{dermal}	9.49E-6	8.87E-6	8.40E-6	7.75E-6	6.40E-6	5.31E-6	1.70E-6	1.59E-6	1.65E-6	1.64E-6	1.63E-6	1.57E-6	1.48E-6
		(3.90E-6)	(3.44E-6)	(3.21E-6)	(2.85E-6)	(2.26E-6)	(1.89E-6)	(5.98E-7)	(5.61E-7)	(5.88E-7)	(5.74E-7)	(5.79E-7)	(5.56E-7)	(5.17E-7)
	THQ	3.26E-4	5.11E-4	4.21E-4	3.14E-4	1.84E-4	1.05E-4	8.08E-5	3.69E-5	3.71E-5	3.68E-5	3.69E-5	3.68E-5	3.68E-5
		(1.32E-4)	(1.95E-4)	(1.59E-4)	(1.14E-4)	(6.50E-5)	(3.77E-5)	(2.87E-5)	(1.35E-5)	(1.38E-5)	(1.34E-5)	(1.36E-5)	(1.35E-5)	(1.33E-5)
Cu	HQ_{ing}	4.31E-4	7.00E-4	6.06E-4	4.15E-4	2.50E-4	1.34E-4	1.07E-4	4.87E-5	4.96E-5	5.09E-5	4.94E-5	4.94E-5	5.02E-5
		(9.69E-4)	(1.69E-3)	(1.52E-3)	(8.68E-4)	(5.90E-4)	(2.90E-4)	(2.58E-4)	(1.20E-4)	(1.21E-4)	(1.39E-4)	(1.05E-4)	(1.08E-4)	(1.22E-4)
	HQ_{dermal}	1.29E-5	1.24E-5	1.23E-5	1.05E-5	9.03E-6	7.08E-6	2.31E-6	2.19E-6	2.31E-6	2.36E-6	2.27E-6	2.20E-6	2.11E-6
		(2.88E-5)	(3.10E-5)	(3.05E-5)	(2.21E-5)	(2.14E-5)	(1.53E-5)	(5.61E-6)	(5.30E-6)	(5.56E-6)	(6.18E-6)	(4.72E-6)	(4.71E-6)	(5.06E-6)
	THQ	4.44E-4	7.12E-4	6.18E-4	4.26E-4	2.59E-4	1.41E-4	1.10E-4	5.09E-5	5.19E-5	5.33E-5	5.17E-5	5.16E-5	5.23E-5
		(9.97E-4)	(1.72E-3)	(1.55E-3)	(8.90E-4)	(6.11E-4)	(3.06E-4)	(2.64E-4)	(1.26E-4)	(1.27E-4)	(1.46E-4)	(1.09E-4)	(1.12E-4)	(1.27E-4)
Pb	HQ_{ing}	4.86E-3	7.86E-3	6.64E-3	4.87E-3	2.78E-3	1.56E-3	1.23E-3	5.42E-4	5.53E-4	5.70E-4	5.73E-4	5.56E-4	5.57E-4
		(5.29E-3)	(8.03E-3)	(7.03E-3)	(5.10E-3)	(2.86E-3)	(1.75E-3)	(1.26E-3)	(5.64E-4)	(6.01E-4)	(6.29E-4)	(6.16E-4)	(5.98E-4)	(5.99E-4)
	HQ_{dermal}	1.45E-4	1.39E-4	9.09E-5	1.23E-4	1.00E-4	8.28E-5	2.64E-5	2.44E-5	2.56E-5	2.66E-5	2.64E-5	2.47E-5	2.34E-5
		(1.58E-4)	(1.43E-4)	(1.45E-4)	(1.30E-4)	(1.02E-4)	(9.12E-5)	(2.71E-5)	(2.49E-5)	(2.75E-5)	(2.92E-5)	(2.81E-5)	(2.62E-5)	(2.50E-5)
	THQ	4.99E-3	8.05E-3	6.80E-3	5.01E-3	2.89E-3	1.65E-3	1.26E-3	5.67E-4	5.78E-4	5.95E-4	6.00E-4	5.81E-4	5.80E-4
		(5.32E-3)	(8.59E-3)	(7.45E-3)	(5.34E-3)	(3.02E-3)	(1.74E-3)	(1.32E-3)	(6.00E-4)	(6.14E-4)	(6.40E-4)	(6.54E-4)	(6.24E-4)	(6.14E-4)
	Ca-ing	1.44E-8	2.34E-8	1.97E-8	1.45E-8	8.28E-9	4.65E-9	3.65E-9	1.61E-9	1.65E-9	1.70E-9	1.71E-9	1.66E-9	1.66E-9
		(1.57E-8)	(2.39E-8)	(2.09E-8)	(1.52E-8)	(8.50E-9)	(5.20E-9)	(3.76E-9)	(1.68E-9)	(1.79E-9)	(1.87E-9)	(1.83E-9)	(1.78E-9)	(1.78E-9)
	$Ca\text{-}_{ihl}$	6.11E-8	6.20E-8	6.34E-8	6.30E-8	6.18E-8	6.21E-8	6.15E-8	6.07E-8	6.18E-8	6.37E-8	6.41E-8	6.21E-8	6.23E-8
		(6.46E-8)	(6.35E-8)	(6.69E-8)	(6.56E-8)	(6.25E-8)	(6.86E-8)	(6.35E-8)	(6.20E-8)	(6.62E-8)	(7.00E-8)	(6.81E-8)	(6.56E-8)	(6.67E-8)
	TCa	7.56E-8	8.54E-8	8.32E-8	7.75E-8	7.01E-8	6.67E-8	6.51E-8	6.23E-8	6.35E-8	6.54E-8	6.58E-8	6.38E-8	6.39E-8
		(8.00E-8)	(8.70E-8)	(8.77E-8)	(8.07E-8)	(7.09E-8)	(7.38E-8)	(6.72E-8)	(6.36E-8)	(6.80E-8)	(7.19E-8)	(7.00E-8)	(6.73E-8)	(6.85E-8)
Cd	HQ_{ing}	4.73E-3	7.60E-3	6.14E-3	4.58E-3	2.65E-3	1.47E-3	1.19E-3	5.26E-4	5.30E-4	5.27E-4	5.30E-4	5.33E-4	5.30E-4
		(2.87E-3)	(4.43E-3)	(3.51E-3)	(2.63E-3)	(1.50E-3)	(8.43E-4)	(6.80E-4)	(3.01E-4)	(3.01E-4)	(3.03E-4)	(3.08E-4)	(3.09E-4)	(3.01E-4)
	HQ_{dermal}	5.68E-3	5.37E-3	4.99E-3	4.64E-3	3.82E-3	3.12E-3	1.02E-3	9.47E-4	9.83E-4	9.83E-4	9.79E-4	9.50E-4	8.91E-4
		(3.45E-3)	(3.15E-3)	(2.88E-3)	(2.67E-3)	(2.16E-3)	(1.78E-3)	(5.80E-4)	(5.31E-4)	(5.49E-4)	(5.52E-4)	(5.57E-4)	(5.39E-4)	(4.97E-4)
	HQ_{ihl}	1.41E-1	1.42E-1	1.40E-1	1.41E-1	1.40E-1	1.39E-1	1.42E-1	1.40E-1	1.41E-1	1.40E-1	1.41E-1	1.42E-1	1.42E-1
		(7.99E-2)	(7.97E-2)	(7.74E-2)	(7.97E-2)	(7.87E-2)	(7.91E-2)	(8.06E-2)	(7.85E-2)	(7.86E-2)	(7.87E-2)	(8.02E-2)	(8.04E-2)	(7.87E-2)
	THQ	1.51E-1	1.55E-1	1.51E-1	1.50E-1	1.47E-1	1.44E-1	1.44E-1	1.42E-1	1.43E-1	1.42E-1	1.43E-1	1.43E-1	1.43E-1
		(8.59E-2)	(8.69E-2)	(8.37E-2)	(8.49E-2)	(8.21E-2)	(8.17E-2)	(8.24E-2)	(7.95E-2)	(8.03E-2)	(7.96E-2)	(8.06E-2)	(8.09E-2)	(8.11E-2)
	$Ca\text{-}_{ihl}$	2.54E-6	2.56E-6	2.51E-6	2.54E-6	2.52E-6	2.51E-6	2.55E-6	2.52E-6	2.54E-6	2.53E-6	2.54E-6	2.56E-6	2.55E-6
		(1.44E-6)	(1.43E-6)	(1.39E-6)	(1.43E-6)	(1.42E-6)	(1.42E-6)	(1.45E-6)	(1.41E-6)	(1.41E-6)	(1.42E-6)	(1.44E-6)	(1.45E-6)	(1.42E-6)

Note: $Ca\text{-}_{ihl}$: inhalation cancer risk, and $Ca\text{-}_{ing}$: ingestion cancer risk.

quantity declined by getting away from the city center, indicating its amount is mainly affiliated to vehicle emissions (Al-Masri et al., 2006; Kemp, 2002). However, the higher Cd amounts were detected in the suburbs (Figs. S4 and S5 of Supplemental materials). Considering the land uses of these areas (Fig. 1), it was revealed that industrial towns and large factories such as steel, ceramic and tile, etc. are dominant there, which can release these pollutants to the atmosphere.

3.2. Risk assessment

By taking into account the risk of selected HMs on both human health and ecological system, the risk assessment accuracy can be significantly improved.

3.2.1. Human health risk

Despite some elements such as Cu and Zn are essential nutrients for human body; the presence of HMs in the polluted air can have serious impacts on health. The assessment results of probabilistic risk as both noncarcinogenic hazard (HQ) and carcinogenic risk (Risk) for each HM and various risk factors in different age groups are shown in Table 2. Based on the total HM contents, the mean HQ values of all HMs in whole age groups were lower than the allowed level ($HQ < 1$). However, the highest HQ belonged to Cd (1.55×10^{-1}), which is close to the threshold. About Zn, Cu, and Pb, the possibility of transferring into the body through oral ingestion is more than dermal absorption ($HQ_{ing} > HQ_{dermal}$), while in the case of Cd, it is more likely to enter the body through inhalation than other pathways ($HQ_{inh} > HQ_{ing}$ and HQ_{dermal}). Furthermore, the mean HQ of each HM for multi-pathway exposure was Cd (1.46×10^{-1}) $\gg$ Pb (2.63×10^{-3}) > Zn (1.66×10^{-4}) > Cu (2.40×10^{-4}).

According to toxicological profiles of Zn, Cu, Pb, and Cd (USDoE, 2011), all these elements have toxicological health effect, but some of them have carcinogenic risk (Cd and Pb). Chabukdhara and Nema (2013) claimed that the order of non-cancer risk of metals in the atmosphere in adult and children was as: Cr > Pb > Mn > Ni > Cu > Cd.

The carcinogenic risk of HMs in the study area is also presented in Table 2. As shown, the carcinogenic risk of Cd in all age groups was higher than the allowed level ($TCR > 1 \times 10^{-6}$), while about Pb, it was in the safe level. Previous studies indicated that HMs could act as a catalyst in oxidative reactions of biological metabolism (Ercal et al., 2001). Therefore, the toxicity of HMs on the body could be due to oxidative tissue damage. The main possible mechanisms of HMs in the body are changing in thiol status, damaging cellular defence system, increasing lipid peroxidation and producing reactive oxygen species (Ercal et al., 2001; Jomova and Valko, 2011). Those cells are under oxidative stress of HMs display various dysfunctions due to damage arising by reactive oxygen species to proteins, lipids and DNA (Ercal et al., 2001; Rehman et al., 2018).

The parameters that influence in the model were determined through sensitivity analysis (Table 3). The results indicated that HMs concentration is the most important variable that affects health risk (Spearman's rank correlation coefficient (r) was ranged between 0.87 and 1.00 for different HMs and age groups). There was a negative correlation between body weight (BW) and estimated risk of each HM (r ranged from 0.00 to - 0.39 for multiple age groups).

The health risk estimated of exposure to Zn, Cu, Pb, and Cd in different age groups should be underestimated. Two reasons can affect this: 1) Although the risk assessment of exposure to ambient HMs was carried out for several exposure pathways (ingestion, inhalation, and dermal exposure), but HMs can enter the body through foods (Clemens and Ma, 2016; Miri et al., 2017a; Real et al., 2017) and water (Fallahzadeh et al., 2018) as well, which not investigated in our study. 2) We further surveyed the HMs concentration in barks as an indicator of HMs pollution in the ambient air of the city; however, all HMs in the air cannot be absorbed into tree barks (Sawidis et al., 2011).

3.2.2. Ecological risk

The potential ecological risk coefficient (E_r^i) and ecological risk index (RI) of air HMs in Yazd area are shown in Fig. 2 and Fig. 3, respectively. The E_r^i values of Zn in all locations were lower than 40, indicated this HM had low ecological risk in the study area. The main element causing potential ecological risk was Cd with moderate to very high ecological risk in most of the study areas, especially in southern and northern regions.

Since more than 350 industries are included in Yazd, therefore, the presence of Cd could be attributed to both traffic and industrial activities (Pongpiachan and Iijima, 2016; Suvarapu and Baek, 2017). These are located in the countryside, i.e., as far as the city center goes towards the suburb, the higher industrial emissions are expected. Pb demonstrated moderate eco-risk on the average, but some crowded central points have a high-risk potential (Fig. 2). In a study by Qing et al. (2015) in China, Cd had the highest ecological risk potential between measured HMs in an urban area. Islam et al. (2015) measured different HMs in urban soils of Bangladesh and reported that Cd had the highest potential ecological risk for the study area. In another study by Sakizadeh et al. (2018) in soil, desert-adapted, and non-desert plants in central Iran, Cd had highest environmental risk. The results of these studies are in line with the finding of the present study.

Moreover, computed RI indices showed moderate to considerable potential ecological risk ($94 \leq RI < 376$) in most of the sampling locations. Based on Fig. 3, higher RI values were found in central parts of the city, near industrial clusters, roadsides, or dumping sites. Hence, the air around the polluted areas is more likely to be exposed to further ecological contaminants and ultimately may cause serious health problems to the residents (Cao et al., 2014).

As a result, this information about the Yazd polluted area shows the necessity to enforce reduction interventions associated with HMs.

3.3. Source identification

3.3.1. Spatial autocorrelation

HM concentration in perimeter air is significantly influenced by spatial and temporal variables, such as climate change, traffic intensity, distance from the road, and resources. Therefore, the specificity and position of each of measured points can be provided. There are several clustering methods for homogeneous data clustering. Among these, Moran's I is of the most commons (Chu et al., 2015; Fang et al., 2016). Here, all HMs in bark samples rendered the negative Moran's indices, representing the scattering of neighbouring points. Given the z-score of Zn (Z-score = −0.728, P-value = 0.466), Cu (Z-score = −0.012, P-value = 0.990), Pb (Z-score = −0.312, P-value = 0.755) and Cd (Z-score = −0.484, P-value = 0.627) the pattern does not appear to be significantly different than random (Table 4). This might be because of high variation of metal content among sampling points in Yazd city from traffic volume and industrial activities at each point. Tepanosyan et al. (2019) used local Moran's I to identify spatial clusters and hot spots of Pb, Mo, and Ti in urban soils of Yerevan, and reported that there was a clustering distribution about Pb concentration and built-up urban areas, and spatially correlated with the wind direction. Similar findings were found in the study of Khosravi et al. (2018), who investigated HMs in urban topsoil. They also reported that industrial activities have a high impact on HMs spatial distribution in the study area.

3.3.2. Principal component analysis and correlation

For better interpretation, analyzing results and further identifying HMs sources in the bark, the principal component analysis (PCA), suggested by US environmental protection agency (EPA), was also used. PCA transforms a given set of correlation variable into the reduced set so that the variable which has the highest variance is the first principal component and one that has the smallest variance is not related to the previous principal (Alahabadi et al., 2017; Guo et al., 2018). In air

Table 3
Sensitivity analysis of carcinogenic and non-carcinogenic risk of exposure to heavy metals.

Element			Age group												
			Birth to < 1	1 to < 2	2 to < 3	3 to < 6	6 to < 11	11 to < 16	16 to < 21	21 to < 31	31 to < 51	51 to < 61	61 to < 71	71 to < 81	81 and older
Cd	Ca_{ihl}	C	1.00	1.00	1.00	1.00	1.00	1.00	1.00	1.00	1.00	1.00	1.00	1.00	1.00
		IR_{ihl}	0.03	0.00	0.00	0.00	0.00	−0.02	0.00	0.01	0.01	0.01	0.01	0.02	0.00
		BW	−0.01	−0.01	0.01	0.00	0.00	0.01	0.00	0.00	0.00	0.00	0.00	0.01	0.02
	THQ	C	1.00	1.00	1.00	1.00	1.00	1.00	1.00	1.00	1.00	1.00	1.00	1.00	1.00
		IR_{ihl}	0.03	−0.03	0.01	−0.02	0.00	0.00	0.00	0.01	0.01	0.00	0.01	0.02	0.00
		BW	−0.03	−0.01	−0.01	−0.01	0.00	−0.02	0.00	0.00	0.00	0.00	0.00	0.01	−0.01
		SA	0.02	0.00	0.00	0.00	−0.01	0.01	−0.01	0.01	0.00	0.01	0.00	0.00	0.01
		IR_{ing}	0.02	0.00	0.00	0.00	0.00	0.01	0.00	0.00	0.01	0.01	−0.01	0.00	0.00
Pb	Ca_{ihl}	C	1.00	1.00	1.00	1.00	1.00	1.00	1.00	1.00	1.00	1.00	1.00	1.00	1.00
		IR_{ihl}	0.02	0.01	0.02	0.00	0.03	−0.01	−0.02	0.01	0.00	0.01	0.01	0.00	−0.01
		BW	0.00	0.01	0.00	0.00	0.00	0.01	0.00	0.01	−0.02	−0.01	0.01	0.00	−0.01
	Ca_{ing}	C	0.97	0.99	0.99	0.99	1.00	1.00	1.00	0.99	0.99	0.99	0.99	0.99	0.99
		IR_{ing}	0.11	0.07	0.07	0.05	0.06	0.05	0.07	0.11	0.10	0.12	0.11	0.14	0.13
		BW	−0.18	−0.13	−0.12	−0.09	−0.05	−0.02	−0.02	−0.01	−0.04	−0.03	−0.01	−0.02	−0.03
	THQ	C	0.97	0.99	0.99	0.99	1.00	1.00	1.00	0.99	0.99	0.99	0.99	0.99	0.99
		IR_{ihl}	0.02	0.01	0.02	0.00	0.03	−0.01	−0.02	0.01	0.00	−0.01	0.00	0.00	0.00
		BW	−0.18	−0.13	−0.12	−0.09	−0.05	−0.02	−0.02	−0.01	−0.04	−0.03	−0.01	−0.02	−0.03
		SA	−0.01	0.00	0.03	0.00	0.00	0.00	0.01	0.01	0.01	−0.02	0.00	0.01	0.00
		IR_{ing}	0.10	0.07	0.07	0.05	0.06	0.05	0.07	0.10	0.10	0.11	0.11	0.13	0.12
Cu	THQ	C	0.99	0.99	1.00	1.00	1.00	1.00	1.00	1.00	1.00	1.00	1.00	1.00	1.00
		IR_{ihl}	0.00	0.00	0.01	0.00	0.00	0.00	−0.01	0.00	0.00	0.00	0.01	0.00	0.01
		BW	−0.11	−0.09	−0.06	−0.04	−0.05	−0.01	−0.01	−0.02	0.00	−0.02	0.00	−0.02	0.00
		SA	0.01	0.00	0.01	0.01	0.01	0.00	−0.01	0.01	0.00	0.00	0.00	0.00	0.00
		IR_{ing}	0.07	0.04	0.05	0.05	0.02	0.03	0.02	0.08	0.07	0.06	0.07	0.06	0.07
Zn	THQ	C	0.87	0.92	0.94	0.96	0.98	0.99	0.99	0.96	0.96	0.96	0.96	0.96	0.96
		IR_{ihl}	−0.02	−0.01	−0.01	0.01	−0.01	0.00	0.00	0.00	0.00	0.00	0.00	0.01	0.00
		BW	−0.39	−0.35	−0.29	−0.20	−0.12	−0.07	−0.05	−0.06	−0.07	−0.06	−0.03	−0.04	−0.04
		SA	0.01	−0.02	0.00	0.01	0.00	0.01	0.00	−0.01	0.00	0.01	0.02	0.01	0.01
		IR_{ing}	0.24	0.14	0.13	0.12	0.14	0.13	0.12	0.26	0.27	0.27	0.27	0.27	0.26

Note: C: concentration of HMs (mg kg^{-1}, or mg m^3), IR_{ihl}: Inhalation rate (m^3 day^{-1}), IR_{ing}: Ingestion rate (mg day^{-1}), BW: Body weight (kg), SA: Total body skin surface area (m^2), Ca_{-ihl}: inhalation cancer risk, and Ca_{-ing}: ingestion cancer risk.

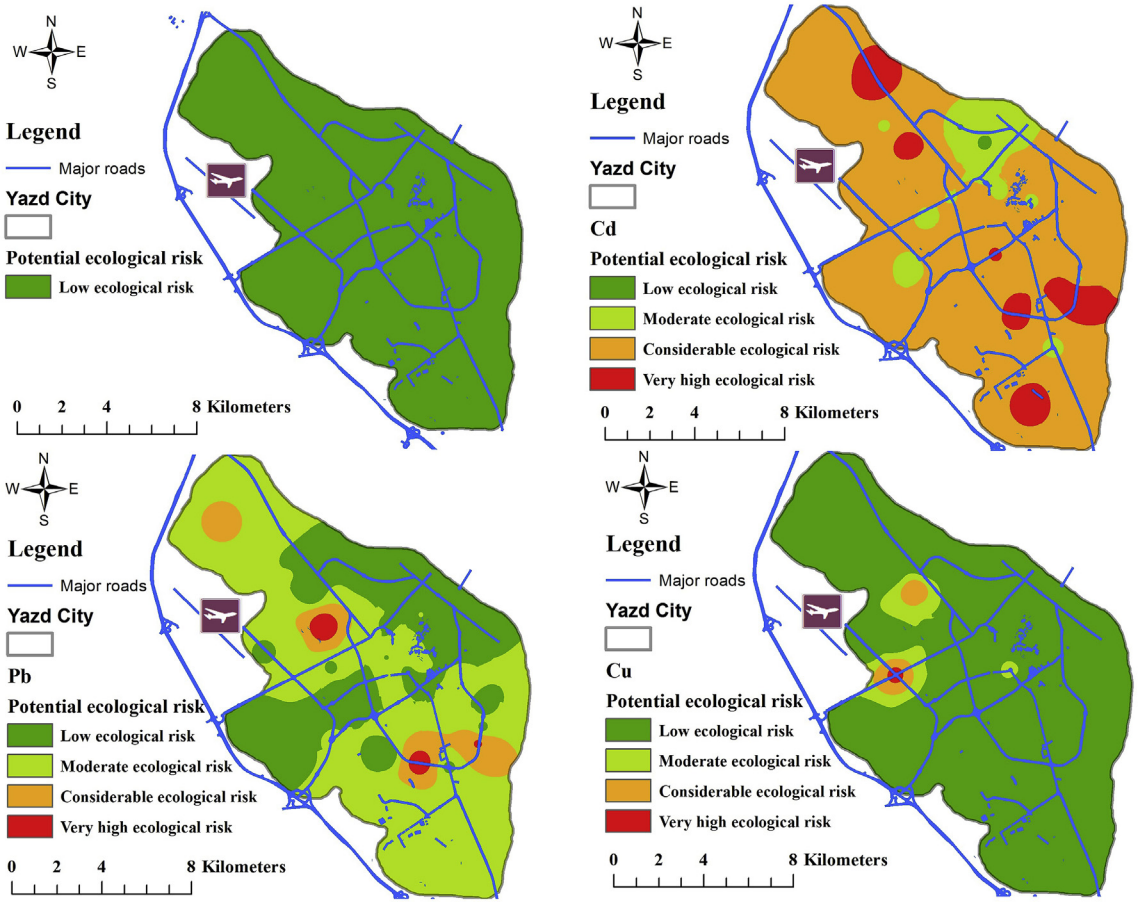

Fig. 2. Potential ecological risk coefficient (E_r^i) of every HM in the study area.

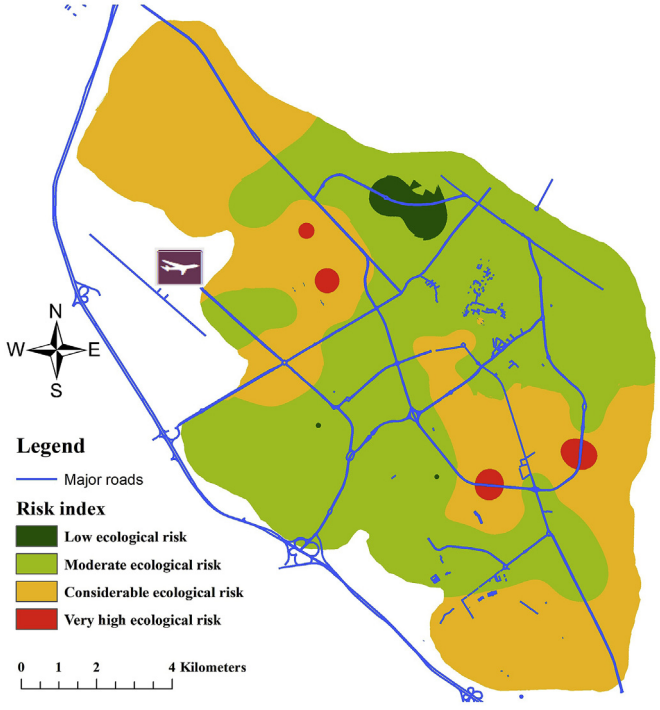

Fig. 3. Ecological risk index (RI) of HMs in the study area.

Table 4
Spatial autocorrelations (Moran's Index) of different heavy metals in study area.

Parameter	Moran's index	Z-score	P-value	Distribution pattern
Zn	−0.075	−0.728	0.466	Random
Cu	−0.022	−0.012	0.990	Random
Pb	−0.042	−0.312	0.755	Random
Cd	−0.055	−0.484	0.627	Random

pollution studies, this method can be used to determine the probable source of the air pollutant (de Souza et al., 2018; Li et al., 2018a; Sun and Sun, 2017). For example, Liang et al. (2016) and Li et al. (2018b) used this technique to detect the source of atmospheric pollutant sources.

Table S2 shows the efficiency of the PCA method and three-factor loadings of metals and their variances. The first component (PC1), which accounted for 36.55% of the total variance, was positively dominated by Cd, Pb, Cu, and Zn, respectively. This group is primarily characterized by to resuspension of road dust (Pb, Cu) and wear-out of brakes and tires (Cu and Zn), especially on express roads (Allajbeu et al., 2017). Cd concentrations were exceptionally higher in PC1; therefore, it may take influence from the point anthropogenic source. Barker and Pilbeam (2015) reported ferrous-steel industries were the major source of environmental Cd contamination. Similar results were documented in some studies, and possible sources have been linked to vehicular emissions (Bowatte et al., 2015; Chabukdhara and Nema, 2013; Moreira et al., 2016; Sadovska, 2012).

In the current study, in addition to traffic emissions, these metals may be particularly linked to industrial pollution, because Yazd city is an industrial area and many manufacturers such as casting, tiling,

textile, electroplating industries, etc. are dominant there. Therefore, Lead-reprocessing units may be responsible for the anthropogenic source of Pb in the region. Zn and Cu showed low positive loadings in PC1, indicating mixed sources for these metals. The second component (PC2) that explained 26.44% of the whole variance showed moderate positive loadings for Cu and Zn, indicating the different anthropogenic source. Whereas, third component (PC3) explained 23.05% of the total variance also indicating robust positive loading for Zn. Zn showed strong relative loadings in PC3, and it may have its contribution from natural sources beside its influence from anthropogenic sources. Dai et al. (2018) investigated the source of HMs in the Poyang lake sediment in China and found that Cr, Pb, and Zn were mainly lithographic and human activities, such as atmospheric transport and rivers, while Cu and Cd can result mainly from human resources such as mining activities and fertilizer application. According to Carvalho-Oliveira et al. (2017), the presence of Cu and Zn in tree bark is an indicator of anthropogenic emissions such as motor vehicles, fossil fuel combustion, and industrial emissions.

The results of Spearman's correlations of HMs in the barks are shown in Table S3. There were low positive correlations (less than 0.402) between all HMs. The highest significant correlation ($r = 0.402$) was found between Zn and Cu, while there was the lowest one ($r = 0.148$) between Pb and Zn. Since the significantly correlated coefficients show more likely the same sources of pollution (Barkett and Akün, 2018; Lu et al., 2010), these results suggest that sampling locations were impressed by different sources of contamination such as vehicles, mining, petrochemical industries, etc. Only Zn and Cu had a significant correlation ($p < 0.01$), and at the best condition, the probability that Cu and Zn had same sources was about 40.2%. Exploring the literature regarding the biomonitoring of atmospheric HMs using local trees reveals indecisive conclusions. Chabukdhara and Nema (2013) have shown vehicle emissions to be the principal source of Pb, Zn in urban environments, while Barkett and Akün (2018) attributed it to the mining operations and atmospheric depositions.

3.3.3. Linear regression model

Results of the relationship between HMs concentration and main traffic indicators (distance from sampling points to the nearest major road, and total road length in a 100, 300 and 500 m buffer around the sampling locations) are shown in Table S4 of Supplemental materials. Accordingly, there was a significant association between Pb and Cu concentration and distance to the nearest highway ($P < 0.05$). By increasing each 1 m distance from highway, the Cu concentration was associated with 0.026 (95% confidence interval (CI): 0.001, 0.052), and about Pb was associated with - 0.011 (95% CI: 0.022, −0.0001) decrease in concentration. There was not a significant association between distance from sampling points to major roads and Cd and Zn concentrations in the bark of trees. Further, total road length in a 100, 300, and 500 m indicated there were no remarkable associations with Zn, Cu, Pb, and Cd concentrations in bark samples. These values suggested that the Pb concentrations in Yazd air were extensively influenced by traffic volume, while a series of sources such as industrial and mining activities, as well as vehicles are involved in the release of these pollutants. Birke et al. (2018) asserted that the outer tree bark collects a considerable amount of particulate matter containing Pb from anthropogenic sources owing to the long exposure time.

4. Conclusion

Our findings of health risk assessment of long-term exposure to HMs indicated that carcinogenic risk of Cd in all age groups was higher than the allowed level. However, the mean values of noncarcinogenic risks of all HMs in whole age groups were in safe level ($HQ < 1$). The main element causing potential ecological risks was Cd, indicating moderate to very high risk in most parts of the study areas. Due to the high concentration of Cd in the study area and high toxicity of this pollutant, emission sources and possible technique for reducing it should be more considered in future studies. Combining different techniques used here can provide higher accuracy in interaction health effect and risk assessment of HMs pollution data, and can help to decision-makers to improve their planning of urbanization. Nevertheless, more researches are required in this field for better understanding and formulation of drastic protective measures for mitigation of the harmful effects of the HMs in the urban atmosphere.

Acknowledgement

The authors are grateful to express their special thanks to the Shahid Sadoughi University of Medical Sciences (SSU) for supporting this project.

Appendix A. Supplementary data

Supplementary data to this article can be found online at https://doi.org/10.1016/j.ecoenv.2019.109622.

References

Bowatte, G., et al., 2015. The influence of childhood traffic-related air pollution exposure on asthma, allergy and sensitization: a systematic review and a meta-analysis of birth cohort studies. Allergy 70, 245–256.
Al-Masri, M.S., et al., 2006. Speciation of Pb, Cu and Zn determined by sequential extraction for identification of air pollution sources in Syria. Atmos. Environ. 40, 753–761.
Alahabadi, A., et al., 2017. A comparative study on capability of different tree species in accumulating heavy metals from soil and ambient air. Chemosphere 172, 459–467.
Allajbeu, S., et al., 2017. Contamination scale of atmospheric deposition for assessing air quality in Albania evaluated from most toxic heavy metal and moss biomonitoring 10. pp. 587–599.
Antoniadis, V., et al., 2017. Trace elements in the soil-plant interface: phytoavailability, translocation, and phytoremediation–A review. Earth Sci. Rev. 171, 621–645.
Apeagyei, E., et al., 2011. Distribution of heavy metals in road dust along an urban-rural gradient in Massachusetts. Atmos. Environ. 45, 2310–2323.
Barker, A.V., Pilbeam, D.J., 2015. Handbook of Plant Nutrition. CRC press.
Barkett, M.O., Akün, E., 2018. Heavy metal contents of contaminated soils and ecological risk assessment in abandoned copper mine harbor in Yedidalga, Northern Cyprus. Environ. Earth Sci. 77, 378.
Bell, M.L., et al., 2011. Environmental health indicators and a case study of air pollution in Latin American cities. Environ. Res. 111, 57–66.
Birke, M., et al., 2018. Tree bark as a bioindicator of air pollution in the city of Stassfurt, Saxony-Anhalt, Germany. J. Geochem. Explor. 187, 97–117.
Cao, S., et al., 2014. Health risks from the exposure of children to As, Se, Pb and other heavy metals near the largest coking plant in China. Sci. Total Environ. 472, 1001–1009.
Carvalho-Oliveira, R., et al., 2017. Effectiveness of traffic-related elements in tree bark and pollen abortion rates for assessing air pollution exposure on respiratory mortality rates. Environ. Int. 99, 161–169.
Chabukdhara, M., Nema, A.K., 2013. Heavy metals assessment in urban soil around industrial clusters in Ghaziabad, India: probabilistic health risk approach. Ecotoxicol. Environ. Saf. 87, 57–64.
Chen, T.-B., et al., 2005. Assessment of heavy metal pollution in surface soils of urban parks in Beijing, China. Chemosphere 60, 542–551.
Chen, P., et al., 2015. Assessment of heavy metal pollution characteristics and human health risk of exposure to ambient PM2.5 in Tianjin, China. Particuology 20, 104–109.
Chu, H.-J., et al., 2015. Modeling the spatio-temporal heterogeneity in the PM10-PM2. 5 relationship. Atmos. Environ. 102, 176–182.
Clemens, S., Ma, J.F., 2016. Toxic heavy metal and metalloid accumulation in crop plants and foods. Annu. Rev. Plant Biol. 67, 489–512.
Cocozza, C., et al., 2016. Integrated biomonitoring of airborne pollutants over space and time using tree rings, bark, leaves and epiphytic lichens. Urban For. Urban Green. 17, 177–191.
Dai, L., et al., 2018. Multivariate geostatistical analysis and source identification of heavy metals in the sediment of Poyang Lake in China. Sci. Total Environ. 621, 1433–1444.
de Souza, J.B., et al., 2018. Generalized additive models with principal component analysis: an application to time series of respiratory disease and air pollution data. J. R. Stat. Soc. Ser. C Appl. Stat. 67, 453–480.
Dirgawati, M., et al., 2016. Development of Land Use Regression models for particulate matter and associated components in a low air pollutant concentration airshed. Atmos. Environ. 144, 69–78.
Dong, L., Liang, H., 2014. Spatial analysis on China's regional air pollutants and CO 2 emissions: emission pattern and regional disparity. Atmos. Environ. 92, 280–291.
Ercal, N., et al., 2001. Toxic metals and oxidative stress part I: mechanisms involved in metal-induced oxidative damage. Curr. Top. Med. Chem. 1, 529–539.
Dormann, C.F., et al., 2007. Methods to account for spatial autocorrelation in the analysis

of species distributional data: a review. Ecography 30, 609–628.
Fallahzadeh, R.A., et al., 2018. Spatial distribution variation and probabilistic risk assessment of exposure to chromium in ground water supplies; a case study in the east of Iran. Food Chem. Toxicol. 115, 260–266.
Fang, C., et al., 2016. Spatial-temporal characteristics of PM2. 5 in China: a city-level perspective analysis. J. Geogr. Sci. 26, 1519–1532.
Ghaffari, H.R., et al., 2017. Asthma disease as cause of admission to hospitals due to exposure to ambient oxidants in Mashhad, Iran. Environ. Sci. Pollut. Res. 24, 27402–27408.
Gholizadeh, A., et al., 2017. Assessment of corrosion and scaling potential in groundwater resources; a case study of Yazd-Ardakan Plain, Iran. Gr. Water. Sustain. Dev. 5, 59–65.
Gholizadeh, A., et al., 2018. Improved power density and Cr/Pb removal using ozone in a microbial desalination cell. Environ. Chem. Lett. 16, 1477–1485.
Guéguen, F., et al., 2012. Atmospheric pollution in an urban environment by tree bark biomonitoring–Part I: trace element analysis. Chemosphere 86, 1013–1019.
Guo, W., et al., 2010. Pollution and potential ecological risk evaluation of heavy metals in the sediments around Dongjiang harbor, Tianjin. Procedia Environ. Sci. 2, 729–736.
Guo, X., et al., 2018. Evaluation of hierarchically weighted principal component analysis for water quality management at Jiaozuo mine. Int. Biodeterior. Biodegrad. 128, 182–185.
Gupta, S., et al., 2016. Lichen as bioindicator for monitoring environmental status in Western Himalaya, India. Int. J. Environ. 5, 1–15.
Hakanson, L., 1980. An ecological risk index for aquatic pollution control.a sedimentological approach. Water Res. 14, 975–1001.
Hirshon, J.M., et al., 2008. Elevated ambient air zinc increases pediatric asthma morbidity. Environ. Health Perspect. 116, 826–831.
Huang, D., et al., 2017. Probabilistic risk assessment of Chinese residents' exposure to fluoride in improved drinking water in endemic fluorosis areas. Environ. Pollut. 222, 118–125.
Islam, S., et al., 2015. Potential ecological risk of hazardous elements in different land-use urban soils of Bangladesh. Sci. Total Environ. 512–513, 94–102.
Janta, R., Chantara, S., 2017. Tree bark as bioindicator of metal accumulation from road traffic and air quality map: a case study of Chiang Mai, Thailand. Atmos. Pollut. Res. 8, 956–967.
Janta, R., et al., 2016. Levels of road traffic heavy metals in tree bark layers of Cassia fistula tree. Int. J. Environ. Sustain. Dev. 7, 385.
Jomova, K., Valko, M., 2011. Advances in metal-induced oxidative stress and human disease. Toxicology 283, 65–87.
Kabata-Pendias, A., 2010. Trace Elements in Soils and Plants. CRC press.
Kanaroglou, P.S., et al., 2013. Estimation of sulfur dioxide air pollution concentrations with a spatial autoregressive model. Atmos. Environ. 79, 421–427.
Kandziora-Ciupa, M., et al., 2016. Accumulation of heavy metals and antioxidant responses in Pinus sylvestris L. needles in polluted and non-polluted sites. Ecotoxicology 25, 970–981.
Kemp, K., 2002. Trends and sources for heavy metals in urban atmosphere. Nucl. Instrum. Methods Phys. Res. Sect. B Beam Interact. Mater. Atoms 189, 227–232.
Keramati, H., et al., 2018. Radon 222 in drinking water resources of Iran: a systematic review, meta-analysis and probabilistic risk assessment (Monte Carlo simulation). Food Chem. Toxicol. 115, 460–469.
Khosravi, Y., et al., 2018. Assessment of spatial distribution pattern of heavy metals surrounding a lead and zinc production plant in Zanjan Province, Iran. Geoderma Reg. 12, 10–17.
Li, H., et al., 2018a. Analyzing the impact of heating emissions on air quality index based on principal component regression. J. Clean. Prod. 171, 1577–1592.
Li, H., et al., 2018b. Investigating the environmental quality deterioration and human health hazard caused by heating emissions. Sci. Total Environ. 628–629, 1209–1222.
Liang, C.S., et al., 2016. Review on recent progress in observations, source identifications and countermeasures of PM2.5. Environ. Int. 86, 150–170.
Lu, X., et al., 2010. Multivariate statistical analysis of heavy metals in street dust of Baoji, NW China. J. Hazard Mater. 173, 744–749.
Luo, X.-S., et al., 2012. Incorporating bioaccessibility into human health risk assessments of heavy metals in urban park soils. Sci. Total Environ. 424, 88–96.
Martin, J.A.R., et al., 2018. Wood and bark of Pinus halepensis as archives of heavy metal pollution in the Mediterranean Region 239. pp. 438–447.
Minganti, V., Drava, G., 2018. Tree bark as a bioindicator of the presence of scandium, yttrium and lanthanum in urban environments. Chemosphere 193, 847–851.
Miri, M., et al., 2016. Ecological risk assessment of heavy metal (HM) pollution in the ambient air using a new bio-indicator. Environ. Sci. Pollut. Res. 23, 14210–14220.
Miri, M., et al., 2017a. Health risk assessment of heavy metal intake due to fish consumption in the Sistan region, Iran. Environ. Monit. Assess. 189, 583.
Miri, M., et al., 2017b. Atmospheric heavy metals biomonitoring using a local Pinus eldarica tree. Health Scope 6.
Miri, M., et al., 2018a. Environmental determinants of polycyclic aromatic hydrocarbons exposure at home, at kindergartens and during a commute. Environ. Int. 118, 266–273.
Miri, M., et al., 2018b. Mortality and morbidity due to exposure to ambient particulate matter. Ecotoxicol. Environ. Saf. 165, 307–313.
Mohsen, M., et al., 2018. Particulate matter concentrations and heavy metal contamination levels in the railway transport system of Sydney, Australia. Transp. Res. D Transp. Environ. 62, 112–124.
Moreira, T.C.L., et al., 2016. Intra-urban biomonitoring: source apportionment using tree barks to identify air pollution sources. Environ. Int. 91, 271–275.
Norouzi, S., et al., 2015. Using plane tree leaves for biomonitoring of dust borne heavy metals: a case study from Isfahan, Central Iran. Ecol. Indicat. 57, 64–73.
Olawoyin, R., et al., 2018. Index analysis and human health risk model application for evaluating ambient air-heavy metal contamination in Chemical Valley Sarnia. Ecotoxicol. Environ. Saf. 148, 72–81.
Parmar, T.K., et al., 2016. Bioindicators: the natural indicator of environmental pollution. Front. Life Sci. 9, 110–118.
Pongpiachan, S., Iijima, A., 2016. Assessment of selected metals in the ambient air PM10 in urban sites of Bangkok (Thailand). Environ. Sci. Pollut. Res. 23, 2948–2961.
Qing, X., et al., 2015. Assessment of heavy metal pollution and human health risk in urban soils of steel industrial city (Anshan), Liaoning, Northeast China. Ecotoxicol. Environ. Saf. 120, 377–385.
Real, M.I.H., et al., 2017. Consumption of heavy metal contaminated foods and associated risks in Bangladesh. Environ. Monit. Assess. 189, 651.
Rehman, K., et al., 2018. Prevalence of exposure of heavy metals and their impact on health consequences. J. Cell. Biochem. 119, 157–184.
Roque-Álvarez, I., et al., 2018. Spatial distribution, mobility and bioavailability of arsenic, lead, copper and zinc in low polluted forest ecosystem in North-western Mexico. Chemosphere 210, 320–333.
Sadovska, V., 2012. Health risk assessment of heavy metals adsorbed in particulates. World Acad. Sci. Eng. Technol. 68, 2151–2158.
Sakizadeh, M., et al., 2018. Trace elements concentrations in soil, desert-adapted and non-desert plants in central Iran: spatial patterns and uncertainty analysis. Environ. Pollut. 243, 270–281.
Sawidis, T., et al., 2011. Trees as bioindicator of heavy metal pollution in three European cities. Environ. Pollut. 159, 3560–3570.
Şen, A., et al., 2015. Heavy metals removal in aqueous environments using bark as a biosorbent. Int. J. Environ. Sci. Technol. 12, 391–404.
Serbula, S.M., et al., 2012. Assessment of airborne heavy metal pollution using plant parts and topsoil. Ecotoxicol. Environ. Saf. 76, 209–214.
Sponza, D., Karaoğlu, N., 2002. Environmental geochemistry and pollution studies of Aliağa metal industry district. Environ. Int. 27, 541–553.
Sun, W., Sun, J., 2017. Daily PM2. 5 concentration prediction based on principal component analysis and LSSVM optimized by cuckoo search algorithm. J. Environ. Manag. 188, 144–152.
Suvarapu, L.N., Baek, S.O., 2017. Determination of heavy metals in the ambient atmosphere. Toxicol. Ind. Health 33, 79–96.
Tepanosyan, G., et al., 2019. The application of Local Moran's I to identify spatial clusters and hot spots of Pb, Mo and Ti in urban soils of Yerevan. Appl. Geochem. 104, 116–123.
Tipping, M.E., Bishop, C.M., 1999. Probabilistic principal component analysis. J. R. Stat. Ser. Soc. B Stat. Methodol. 61, 611–622.
Uchiyama, R., et al., 2019. Characteristics of trace metal concentration and stable isotopic composition of hydrogen and oxygen in “urban-induced heavy rainfall” in downtown Tokyo, Japan; the implication of mineral/dust particles on the formation of summer heavy rainfall. Atmos. Res. 217, 73–80.
USDoE, 2011. The Risk Assessment Information System (RAIS). US Department of Energy’s Oak Ridge Operations Office (USDoE).
USEPA, 2011. Exposure Factors Handbook, 2011 Edition. National Center for Environmental Assessment, Washington, DC.
Viana, M., et al., 2006. Identification of PM sources by principal component analysis (PCA) coupled with wind direction data. Chemosphere 65, 2411–2418.
Wold, S., et al., 1987. Principal component analysis. Chemometr. Intell. Lab. Syst. 2, 37–52.
Zhao, H., et al., 2012. Human health risk from soil heavy metal contamination under different land uses near Dabaoshan Mine, Southern China. Sci. Total Environ. 417, 45–54.
Zhao, Q., et al., 2014. Potential health risks of heavy metals in cultivated topsoil and grain, including correlations with human primary liver, lung and gastric cancer, in Anhui province, Eastern China. Sci. Total Environ. 470, 340–347.